Magnetic and electronic interaction effects at the interfaces of Fe/V_2O_3 and Co/V_2O_3 bilayers

B. Sass, C. Tusche, and W. Felsch
I. Physikalisches Institut, Universität Göttingen, Friedrich-Hund-Platz 1, 37077 Göttingen, Germany

F. Bertran, F. Fortuna, P. Ohresser, and G. Krill
Laboratoire pour l'Utilisation du Rayonnement Electromagnétique, Bâtiment 209 D, Centre Universitaire Paris-Sud, B.P. 34, 91898 Orsay, France

(Received 28 May 2004; revised manuscript received 9 September 2004; published 12 January 2005)

Thin films of $V_2O_3(11\bar{2}0)$ can exist in metallic and insulating phases with different magnetic properties, similar as the bulk single crystals. We have used macroscopic magnetometry and x-ray absorption spectroscopy together with magnetic circular dichroism to show that when these films are combined with thin overlayers of bcc Fe and hcp Co, this has a pronounced impact on the electronic and magnetic properties of the interfaces. While the uncovered oxide is metallic at room temperature, both ferromagnets induce an insulating phase near the surface of the oxide, presumably due to hybridization effects at the interface. Remarkably, the electronic interaction across the interface is significantly different for the two systems. This is reflected in a magnetically "dead" atomic layer in the Fe films at the interface, a property not observed in the Co films. As a consequence the magnetic anisotropy of the two ferromagnets is dissimilar. In the antiferromagnetic phase of V_2O_3, at $T < T_N \approx 160$ K, the hysteresis loops of the Co films exhibit a significant exchange bias; the effect is absent for Fe. The faceted surface structure of the $V_2O_3(11\bar{2}0)$ layers induces a uniaxial magnetic anisotropy with magnetocrystalline and magnetostatic contributions in both ferromagnetic overlayers.

DOI: 10.1103/PhysRevB.71.014415 PACS number(s): 75.70.Cn, 75.30.Gw, 73.40.Ns, 78.70.Dm

I. INTRODUCTION

Understanding the chemical-physical properties at the interface of a ferromagnetic metal and an insulating oxide in thin-film structures is a central topic of current research activity.[1] The knowledge of interfacial interactions and spin configurations at the microscopic level is of high interest for a variety of magnetic phenomena as, for example, in the context of spin tunnel[2] or exchange biased[3–5] structures, which have potential applications in magneto electronics.[6] Interfacial signatures may be weak, and to detect and isolate them from bulk properties generally is a great challenge. In the last decade progress in the techniques of growth and characterization of thin-film sandwiches that are structured on nanometer length scales has considerably advanced the field; concomitantly, valuable information was gained from the study of systems with increasing complexity.[7]

Here we report on the electronic and magnetic properties of bilayers combining the ferromagnets Fe or Co with single-crystalline $V_2O_3(11\bar{2}0)$. The large variety of unusual physical properties of this oxide has a long history,[8] and is a rich ground for basic research. Strong electron correlations lead to a complex interplay of magnetism, structure, and transport that poses major problems for a theoretical modelling.[9–11] Hybridization of the V 3*d* with the O 2*p* orbitals competes with strong Coulomb interactions within the 3*d* shell (formal configuration $3d^2$). Small perturbations in the balance of these effects induce drastic modifications of the electronic properties. This is manifest in a very rich phase diagram.[12] Stoichiometric V_2O_3 is in a paramagnetic metallic (PM) phase at room temperature and undergoes a first-order transition to an antiferromagnetic insulating (AFI) phase at $T_{MI} = T_N \approx 160$ K, with a band gap of ~ 0.6 eV. Concomitantly, the lattice symmetry transforms from rhombohedral to monoclinic. At temperatures sufficiently above T_{MI}, substitution of V ions by Cr results in the formation of a paramagnetic insulating (PI) phase, which changes to the AFI monoclinic phase near 180 K. The magnetic ordering pattern in the AFI phase is very peculiar and not that of a simple two-sublattice Néel configuration.[13] In the hexagonal basal plane (0001) exchange coupling for each V^{3+} ion is ferromagnetic with one of the neighbors and antiferromagnetic with the other two. This translates to ferromagnetic alignment of the magnetic moments within the $(11\bar{2}0)$ planes with antiferromagnetic coupling of adjacent planes. The moments ($\sim 1.2\ \mu_B$/V ion) form an angle of $\sim 70°$ with the *c* axis located in the $(11\bar{2}0)$ plane. Combining this material with Fe and Co in bilayers offers the unique possibility to study the variation of the interfacial properties of a ferromagnet/oxide system when the oxide is tuned to the metallic, insulating, paramagnetic and antiferromagnetic phases.

We have shown recently that V_2O_3 films of high quality can be grown epitaxially on $(11\bar{2}0)$-oriented sapphire substrates.[14] These films exhibit bulk like properties with good stoichiometry. The surface has a faceted microstructure, which results from the anisotropic lattice mismatch between film and substrate. In this paper, we shall demonstrate that due to this morphology thin films of Fe and Co deposited on the $V_2O_3(11\bar{2}0)$ layers display a pronounced in-plane uniaxial magnetic anisotropy at room temperature. Upon cooling in a magnetic field across the Néel temperature T_N of V_2O_3, the two bilayer systems show a remarkable difference in their magnetic behavior: while the magnetization loops of Co on $V_2O_3(11\bar{2}0)$ exhibit a significant exchange bias effect—i.e., are centered about a nonzero magnetic field H_{EB}—this effect is absent for Fe on $V_2O_3(11\bar{2}0)$. This obser-

vation adds another aspect to the ongoing debate over the microscopic origin of the unidirectional exchange anisotropy in ferromagnets in contact with an antiferromagnet. We use soft x-ray absorption (XA) spectroscopy combined with measurement of x-ray magnetic circular dichoism (XMCD) for electronic and magnetic characterization of the interfaces between Co or Fe and adjoining V_2O_3, taking benefit from the elemental and magnetic sensitivity of this technique and from the interfacial sensitivity of the electron-yield detection mode employed. The XMCD spectra suggest that the absence of the exchange anisotropy in $Fe/V_2O_3(11\bar{2}0)$ may be related to the formation of a magnetically "dead" Fe layer at the interface, a property not observed in the case of $Co/V_2O_3(11\bar{2}0)$. The XA spectra reveal that both ferromagnetic overlayers induce the PI phase in the adjoining V_2O_3 near the interface. This remarkable effect is observed at room temperature where the bare oxide layer is metallic compliant to the phase diagram.[8]

II. EXPERIMENT

V_2O_3 films were grown epitaxially on $(11\bar{2}0)$-oriented sapphire substrates $[\alpha\text{-}Al_2O_3(11\bar{2}0)]$ at 600 °C by reactive dc magnetron sputtering, as described elsewhere.[14] Self-organized growth leads to a stripe-shaped microstructure at the surface. Scanning tunneling microscope (STM) images revealed atomically flat terraces of typical size 200×20 nm^2, elongated perpendicular (in good approximation) to the *c* axis of the rhombohedral corundum structure in the $(11\bar{2}0)$ plane. The overall root-mean-square (rms) roughness varies somewhat with the thickness of the films and is about 1 nm. The surface topology is stable upon repeated cycling of the films across the metal-insulator transition.

For the preparation of the bilayers, Fe and Co were deposited at normal incidence on the $V_2O_3(11\bar{2}0)$ films at ambient temperature, either *in situ* by ion-beam sputtering with Ar in the preparation chamber of our laboratory for superconducting quantum interference device (SQUID) magnetometry (thickness $t_{Fe,Co}$ above 2.5 nm) or *ex situ* by thermal evaporation under UHV conditions (pressure $<10^{-10}$ mbar) using effusion cells in the preparation chamber of the synchrotron beamline for XA spectroscopy ($t_{Fe,Co}$ up to 1 nm). The growth rates were approximately 0.5 Å/s in the first case and 1 Å/min in the second case. The thickness was controlled by a quartz microbalance and, in the case of XA, by the edge jump with an estimated accuracy of 5%. In the latter case, before Fe and Co deposition, a thin overoxidized surface layer of the V_2O_3 films resulting from air exposure was removed by Ar-ion etching, and subsequent annealing at 800 °C restored an ordered $V_2O_3(11\bar{2}0)$ surface. For the *ex situ* magnetization measurements the Fe/V_2O_3 and Co/V_2O_3 bilayers were covered with a ~40-Å-thick protective layer of Al before air exposure.

X-ray Bragg scans recorded along the normal of the bilayers with thickness $t_{Fe,Co} > 2.5$ nm reveal textured growth of Fe with bcc (110) orientation and of Co with hcp (0001) orientation on the $V_2O_3(11\bar{2}0)$ films. Laue oscillations around the related Bragg peaks indicate structural coherence across the entire thickness (Fig. 1). The interfaces are sharp.

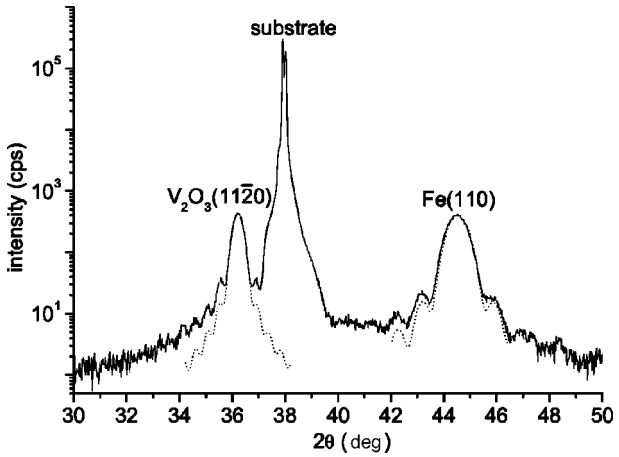

FIG. 1. X-ray diffraction diagram (Cu $K\alpha$ radiation, θ-2θ geometry) measured on a bilayer of 10 nm Fe and 80 nm $V_2O_3(11\bar{2}0)$ around the (110) reflection of Fe and $(11\bar{2}0)$ reflection of V_2O_3. Dotted curves: Simulation of the superstructure reflections using the kinematical scattering theory (interfacial rms roughness: 0.6 nm).

The lattice is slightly expanded (<1%) along the growth direction. This is not surprising in view of the smaller atomic distances in the ferromagnets and points to the presence of compressive strain at the interfaces. Information on the early stage of Fe and Co growth in the ultrathin limit, for $t_{Fe,Co} \leqslant 1$ nm, is only indirectly available from the evolution of the XMCD signals with thickness. The data indicate that the Fe layers grow in a predominantly layer-by-layer mode; they do not permit to draw a definite conclusion on the growth of the Co layers (see below).

The XA spectra were acquired at the soft x-ray beamline SU23 of the SuperACO storage ring at the synchrotron radiation facility LURE in Orsay, France. The beamline supplies a monochromatic beam by a grating spectrometer with a resolution of ~0.6 eV in the energy range of interest (500–900 eV); it results from an asymmetric wiggler and is 65% circularly polarized. Electronic transitions from the V 2*p* and O 1*s* as well as Fe and Co 2*p* states into dipole-allowed unoccupied states with *d* and *p* character, respectively, were studied. The spectra were obtained in an UHV system (base pressure $<10^{-10}$ mbar) by measuring the total electron yield (TEY) and are estimated to sample the top ~2.5 nm of the layers. XMCD experiments probe the absorption cross section at a core-level threshold of a material with a net magnetic moment for two opposite relative orientations of the magnetization and helicity of circularly polarized photons. The difference of the spectra measures the net magnetic moment through transfer of the x-ray angular momentum vector in the absorption process. Due to the creation of a core hole, this technique is site and orbital selective. Here, the XMCD spectra of the Fe and Co layers were recorded *in situ* after their deposition at constant beam helicity by scanning the photon energy across a given absorption edge for two opposite directions of the saturation magnetization induced by applying an external magnetic field (1 T) parallel and opposite to the x-ray propagation direction; it was oriented at an angle of 45° with respect to the layer normal and reversed at each energy point. The XMCD signal

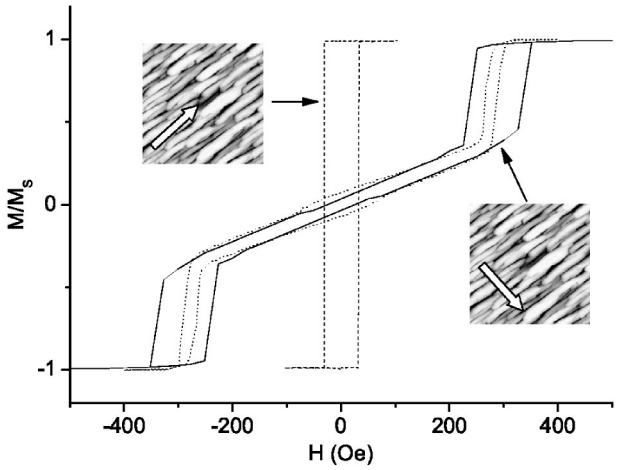

FIG. 2. Hysteresis loop of a Fe layer (thickness 10 nm) on $V_2O_3(11\bar{2}0)$ recorded at 300 K with a SQUID magnetometer. External magnetic field in the layer plane, perpendicular (dashed curve) and parallel (dotted curve) to the V_2O_3 *c* axis. Solid curve: fit of the hard-axis loop by a coherent rotation model [Eq. (1)]. Insets: topographic STM image of the $V_2O_3(11\bar{2}0)$ surface (400×400 nm^2; see Ref. 14) to illustrate the orientation of the external magnetic field (open arrows).

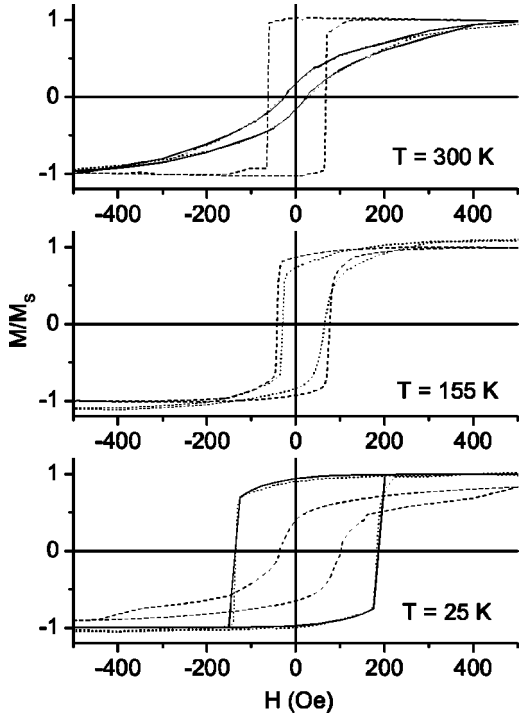

FIG. 3. Hysteresis loop of a Co layer (thickness 5 nm) on $V_2O_3(11\bar{2}0)$ at different temperatures. External magnetic field in the layer plane, perpendicular (dashed curve) and parallel (dotted curve) to the V_2O_3 *c* axis. Sample cooled in a magnetic field of −50 kOe, parallel to field applied for the measurement. The loops recorded parallel to the V_2O_3 *c* axis at 300 K and 25 K are fitted by the coherent rotation model of Eq. (1) together with (at 25 K) Eq. (2) (solid curves).

is the difference between the normalized absorption coefficients for the two field directions. It is important to note that the applied magnetic field is sufficiently strong to warrant magnetic saturation of the Fe and Co layers along its direction in the ultrathin limit, $t_{Fe,Co} \leqslant 1$ nm. This was ascertained by measuring hysteresis curves of the overlayers in situ by using the XMCD technique:[15] a loop recorded at the energy of the peak of the dichroic signal at the Fe and Co L_3 edge, respectively, by varying the external field between ±1 T was corrected for the (magnetic-field dependent) nonmagnetic contribution to the TEY signal by a loop measured just below the edge where no magnetic dichroism is present. We note further that corrections due to saturation effects, in most cases mandatory for XA spectra detected by TEY (Ref. 16) (in particular if orbital magnetic moments are deduced) are not required here; as the thickness of the Fe and Co layers studied was limited to 1 nm, the electron escape length is small compared to the x-ray absorption depth for the chosen experimental geometry. In fact, XA spectra recorded on the 1-nm-thick overlayers for different angles of incidence of the x-ray beam confirmed that saturation effects are negligible here.

III. RESULTS AND DISCUSSION

A. Magnetic anisotropies of Fe and Co overlayers on $V_2O_3(11\bar{2}0)$

The spontaneous magnetizations of Fe and Co on $V_2O_3(11\bar{2}0)$ ($t_{Fe,Co} > 2.5$ nm) measured with a SQUID magnetometer agree with the values of the bulk materials; they vary little with temperature between 4.2 and 300 K. The shape anisotropy keeps them in the layer plane. The faceted, stripe-shaped surface structure of the oxide layer is the source of a pronounced uniaxial in-plane magnetic anisotropy of the ferromagnetic (F) overlayers. This is apparent from the shapes of the magnetization curves $M(H)$ measured with the external magnetic field H applied parallel and perpendicular to the stripes in the layer plane. A representative set of hysteresis loops of both ferromagnets (for Fe at room temperature only) is presented in Figs. 2 and 3. The shape of these loops identifies, at room temperature, the direction parallel to the stripes on the V_2O_3-layer surface—i.e. perpendicular to the rhombohedral *c* axis—as the easy magnetization axis of both F layers. Perpendicular to the stripes, Fe and Co exhibit a hard-axis loop that is distinctly different for the two metals. For Fe a split loop with small remanence is observed (Fig. 2). When the magnetic field applied along the *c* axis is increased from zero first a linear behavior is found, indicating that the magnetization tends to align along the field direction away from the uniaxial easy direction essentially through coherent spin rotation. At a higher field H_s it switches irreversibly to complete alignment with the hard direction in a single jump. In the case of Co the loop shows negative curvature and magnetization alignment along the hard axis is more gradual and governed by spin rotation.

The hard- and easy-axis magnetization curves of the Fe layers on $V_2O_3(11\bar{2}0)$ essentially do not vary down to low temperature. In particular, there is no exchange coupling across the interface to AF V_2O_3 that would be manifest in a displacement of the hysteresis curves on the magnetic-field axis for the samples cooled through the Néel temperature T_N

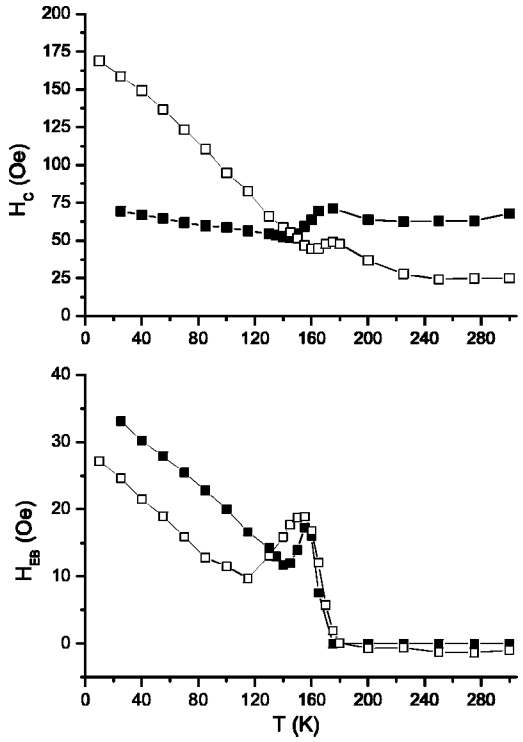

FIG. 4. Exchange-anisotropy field H_{EB} (lower panel) and coercive field H_C (upper panel) of the Co/$V_2O_3(11\bar{2}0)$ bilayer of Fig. 3 as a function of temperature, cooled in a magnetic field of −50 kOe. H_{EB} opposed the direction of the cooling field. Open symbols: measured parallel to the *c* axis of V_2O_3.

in a magnetic field. In contrast, such bias effect is clearly visible in the case of the Co/$V_2O_3(11\bar{2}0)$ bilayers, both for the easy- and hard-axis loops (Fig. 3). This difference is intriguing; it points to drastically different interfacial interactions in the two-bilayer systems. This will be further addressed below. Figure 4 (lower panel) shows the evolution of the bias field H_{EB} with temperature for the sample referred to in Fig. 3. H_{EB} is distinctly larger perpendicular to the V_2O_3 *c* axis than parallel to it. Eye-catching features are the pronounced maximum near the onset of AF order in the oxide layer (Fig. 4) and the asymmetry of the hysteresis loop parallel to the *c* axis just below T_N (at $T=155$ K, Fig. 3). The latter effect mirrors different processes in magnetization reversal on either side of the hysteresis loop and is a frequent observation in exchange-bias systems. Varying the cooling field between 0.5 and 50 kOe had no effect on any of the results. Worthy of note is that the exchange anisotropy is not observed for Co layers grown on a $V_2O_3(11\bar{2}0)$ surface overoxidized by exposure to air. Below T_N the exchange anisotropy at the Co–$V_2O_3(11\bar{2}0)$ interface is superimposed to the anisotropy induced by the anisotropic surface morphology of the oxide. A remarkable result is that the hard and easy axes of magnetization are interchanged: the easy-axis loop at 300 K (measured perpendicular to the V_2O_3 *c* axis) becomes a hard-axis loop below T_N and vice versa. Concomitantly, the coercivity parallel to the *c* axis increases considerably toward low temperature (Fig. 4, upper panel). As the bias fields H_{EB} the coercive fields H_C show maxima around $T_N=T_{MI}$.

In essence, the different anisotropic features observed in magnetization reversal of the Fe and Co films on

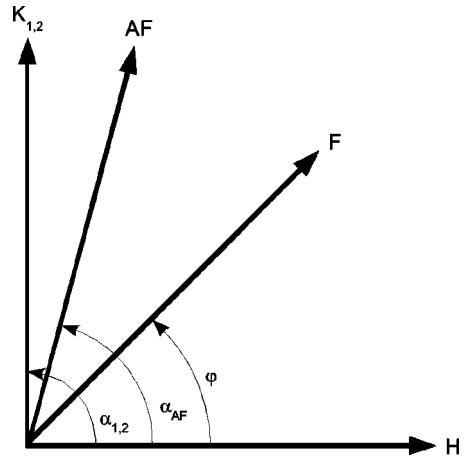

FIG. 5. Angular relations between the directions of the saturation magnetization of the ferromagnetic overlayers (*F*), their magnetic easy axis (labeled by the anisotropy energies $K_{1,2}$), the easy axis of antiferromagnet V_2O_3 (*AF*), and the external magnetic field *H*.

$V_2O_3(11\bar{2}0)$ are not new (except the absence of exchange bias in the Fe films). We first discuss the behavior in the PM regime of V_2O_3. At $T>T_N$, the pertinent micromagnetic mechanisms expected are, besides the usual magnetocrystalline volume anisotropies of Fe and Co, magnetocrystalline and magnetostatic dipolar anisotropies related to the rough anisotropic interface morphology that results from the faceted $V_2O_3(11\bar{2}0)$ surface. Magnetocrystalline anisotropy originates intrinsically from a spin-orbit-based mechanism that depends sensitively on the local lattice symmetry around the moment-carrying ions. The role of broken symmetry (missing bonds) at surfaces and interfaces in magnetic anisotropy[17] was extensively explored on F films grown on stepped surfaces.[18–22] It induces a uniaxial anisotropy within the film plane. This mechanism must be equally relevant for the present bilayer systems. Strain in the F layers due to the lattice mismatch at interfaces may be the source of a volume-type magnetoelastic contribution again with twofold symmetry about the layer normal.[23] Finally, an extrinsic contribution to the uniaxial in-plane anisotropy comes from magnetic stray dipolar fields generated by magnetization fluctuations at the interface with its anisotropic roughness. This mechanism was analyzed by Arias and Mills;[24] its observation is documented in the literature.[25,26] In an external field, if we assume a homogeneous magnetization in the F layers, the (in-plane) anisotropy energetics based on theses mechanisms are contained, at $T>T_N$ of V_2O_3, in the free enthalpy density

$$g_A = -MH\cos\varphi + K_1\sin^2(\alpha-\varphi) + K_2\sin^4(\alpha-\varphi). \quad (1)$$

Here, *M* is the saturation magnetization of the ferromagnets, *H* is the magnetic field applied parallel to the layer plane at an angle φ with the magnetization, K_1 and K_2 are twofold and fourfold anisotropies about the layer normal, respectively, and α is the angle between the applied field and the magnetic easy axis (see Fig. 5). K_2 may denote a second-order contribution of the uniaxial anisotropy and/or, in the case of the cubic Fe overlayers, a magnetocrystalline volume

anisotropy. Equation (1) permits, by minimization of g_A with respect to φ, to model magnetization reversal in the Fe and Co overlayers along the hard axis—i.e., the V_2O_3 *c* axis. As can be seen in Figs. 2 and 3, the essential features of the hysteresis loops $M(H)$ are well described by this Stoner-Wohlfarth-like coherent spin rotation approach, if slightly different orientations $(\alpha_1-\varphi)$ and $(\alpha_2-\varphi)$ of the anisotropies K_1 and K_2 with respect to M are chosen ($\alpha_1=92$ and $\alpha_2=88°$ for Fe, $\alpha_1=80°$ and $\alpha_2=85°$ for Co).[27] This difference may indicate that magnetization reversal is not a simple coherent rotation; domain processes are likely to be operative. Such processes are particularly noticeable in the magnetization loop of Fe near the switching field H_S. The fitted anisotropy constants are $K_1=7.0\times10^5$ erg/cm^3 and $K_2=-3.2\times10^5$ erg/cm^3 for the Fe layer and $K_1=1.2\times10^5$ erg/cm^3 and $K_2=+1.1\times10^5$ erg/cm^3 for the Co layer on $V_2O_3(11\bar{2}0)$. The constants have the same order of magnitude for both F layers; the two systems differ essentially in the sign of the fourfold anisotropy parameter K_2, which in our notation is negative for the Fe and positive for the Co system. In the case of Fe, the twofold anisotropy parameter K_1 is responsible for the initial linear increase of the $M(H)$ loop before it switches to alignment along the V_2O_3 *c* axis due to the competing influence of the fourfold anisotropy $K_2<0$. It is not straightforward to correlate the anisotropy K_2 with an intrinsic fourfold symmetry of the two systems—i.e., with the volume properties of the F overlayer itself or with the interface with the $V_2O_3(11\bar{2}0)$ surface. While in the case of Fe K_2 may be related to the magnetocrystalline volume anisotropy of cubic (bcc) Fe, a similar correspondence is not possible in the case of the Co overlayers in view of their hexagonal (0001) texture.

Inspection of Figs. 2 and 3 [$M(H)$ loop at 300 K] suggests that magnetization reversal in the Fe and Co overlayers along the easy axis—i.e., parallel to the stripes on the V_2O_3-layer surface—essentailly proceeds via domain nucleation and domain-wall propagation processes. No attempts were made to model this behavior. Furthermore, magnetization loops recorded for representative samples with the external magnetic field applied along various different azimuthal angles referred to the stripes (not shown here) display a complex shape due to the superposition of such domain processes and magnetization rotation.[28] Hence such loops do not help to understand magnetization reversal on the Fe and Co overlayers more in detail. It is important to note that the Fe overlayers present almost identical magnetization loops if they are deposited onto the surface of $V_2O_3(11\bar{2}0)$ overoxidized by air exposure, with essentially the same faceted morphology. This means that the direct electronic contact with the stoichiometric oxide is not involved in generating the magnetic anisotropy. This is at variance with the Co adlayers for which the anisotropy is considerably reduced if they are grown on the overoxidized $V_2O_3(11\bar{2}0)$ surface. Hence the anisotropy of the Co layers must be linked basically to the direct electronic interaction at the interface with stoichiometric V_2O_3.

With the advent of AF order in V_2O_3, at $T<T_N$, the magnetic easy axis of the Co overlayers is tilted toward the *c* axis of the oxide, away from the easy direction of the antiferromagnet (Fig. 3). This rotation, as the bias of the hysteresis loop, must be attributed to the exchange coupling across the interface now dominating the magnetic anisotropy. In fact, as first shown by Koon[29] via numerical simulations, exchange coupling of a ferromagnet to the compensated interface of an antiferromagnet (i.e., with zero net moment) leads to a perpendicular orientation between the F/AF easy-axis directions, except for a small canting of the AF spins that generates a net moment in the antiferromagnet parallel to the F magnetization. This is similar to the spin-flop state of a bulk antiferromagnet in an external magnetic field. The coupling gives rise to a uniaxial anisotropy in the ferromagnet.[30] A key issue for the additional appearance of exchange bias—i.e., of a unidirectional anisotropy—in such systems is the formation of a partial domain wall in the antiferromagnet near the interface upon rotation of the F magnetization.[31,5] In the present system, the ideally uncompensated $(11\bar{2}0)$ surface of AF V_2O_3 is likely to be compensated or partially compensated on average, since because of the faceted surface of the layers both sublattices of the antiferromagnet will be exposed. Hence, similarly as in the model of Koon,[29] the spins in the interface region are frustrated by competing exchange interaction between the two sublattices of the antiferromagnet and the ferromagnet. The F/AF exchange coupling adds a contribution

$$\Delta E = + J_{F/AF}\cos(\alpha_{AF}-\varphi) + J_{1,F/AF}\cos^2(\alpha_{AF}-\varphi) \quad (2)$$

to the free enthalpy of the F layers in Eq. (1), where $J_{F/AF}$ and $J_{1,F/AF}$ are constants denoting the unidirectional and uniaxial exchange-induced anisotropies and α_{AF} is the angle between the applied field and the AF easy axis. The quadratic term competes with the uniaxial term in Eq. (1). The free enthalpy in Eq. (1) with the supplement of the contribution in Eq. (2) is used to model magnetization reversal in Co on $V_2O_3(11\bar{2}0)$ at 25 K with the magnetic field applied along the *c* axis of the oxide. A good representation of the measured $M(H)$ loop is obtained (Fig. 3) with the anisotropy parameters K_1, K_2, α_1, and α_2 determined by the fit to the room-temperature loop and F/AF exchange-induced anisotropies $J_{F/AF}=-4.5\times10^4$ erg/cm^3 and $J_{1,F/AF}=3.8\times10^5$ erg/cm^3 and the angle $\alpha_{AF}=90°$. Let us note that detailed magnetization processes are not in the focus of this study. Hence domain processes and a possible temperature dependence of K_1 and K_2 are ignored. The essential result is that exchange coupling of Co to the surface of adjacent AF $V_2O_3(11\bar{2}0)$ favors the Co magnetic moments being perpendicular to the magnetic moments of V_2O_3. This perpendicular coupling dominates the magnetic response. In fact, comparison with the $M(H)$ loop perpendicular to the V_2O_3 *c* axis illustrates that the Co magnetic easy axis switches by $\sim90°$ if T is varied across T_N. A similar rotation of the F easy axis was previously observed for an exchange-biased Fe film on Cr(001) where the uncompensated Cr(001) surface can be partially compensated by the presence of random steps.[32]

B. Microscopic properties of Fe, Co, and V in Fe(Co)/$V_2O_3(11\bar{2}0)$ bilayers

We now focus on the spontaneous magnetic moments of the Fe and Co overlayers on $V_2O_3(11\bar{2}0)$ in the ultrathin

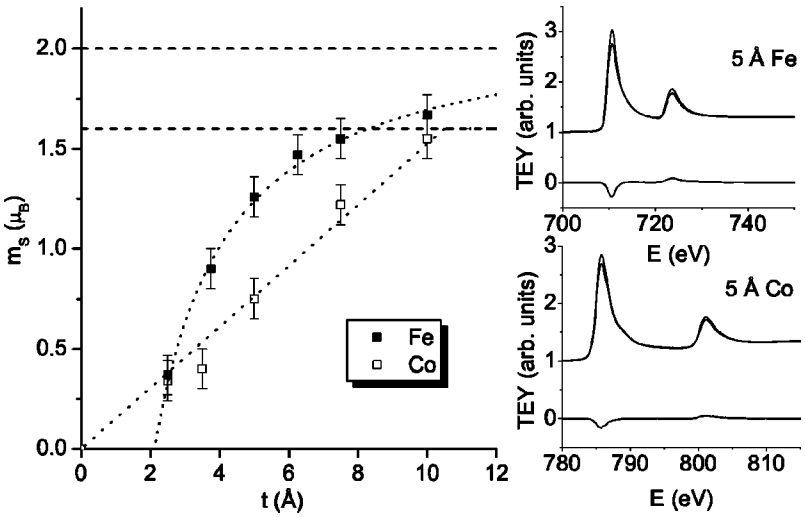

FIG. 6. Right panel: XA and XMCD spectra [$L_{2,3}(2p \rightarrow 3d)$ edges] of ultrathin Fe and Co layers on $V_2O_3(11\bar{2}0)$: left panel: average magnetic spin moments per Fe and Co atom, m_S, as a function of coverage $t_{Fe,Co}$ at 290 K. The same values of m_S are observed at 10 K within the experimental error. The dotted curves are a guide to the eye (Co) or represent the functional form given in the text. Dashed horizontal lines: values of the bulk spin moments of Fe and Co.

regime ($t_{\mathrm{Fe,Co}} \leqslant 1$ nm), measured by XMCD. Typical XA and XMCD spectra measured at the $L_{2,3}$ edges of these elements are shown in Fig. 6 (right panels). The isotropic XA spectra clearly reveal the character of Fe and Co metal; i.e., we can exclude an eventual formation of Fe oxide or Co oxide at the interface with V_2O_3, which would impose their signature on the spectral shape.[33] This is an important point. The magneto-optical sum rules[34] were used to extract the spin and orbital magnetic moments from the XMCD spectra. In order to separate the transition to empty 3*d* states ("white line") from other allowed transitions, a simple two-step function was subtracted from the isotropic XA spectra normalized before the edge. The number of 3*d* holes was set to 3.39 for Fe and 2.49 for Co.[35] The left panel of Fig. 6 presents the thickness variation of the mean magnetic spin moment per Fe and Co atom, $m_S(t_{\mathrm{Fe,Co}})$, at room temperature. No significant variation of these moments was noticed when the temperature was decreased to 10 K even for the lowest thickness, indicating that the Curie temperature of the layers is higher than room temperature. We note that the orbital magnetic moments amounts to roughly 5% and 10% of the spin moments of Fe and Co, respectively, and follow the same trend in the variation with the overlayer thickness as the spin moment. But because of the relatively large error bars, details will not be regarded here. Furthermore, the dipolar magnetic contribution to the spin moment is neglected, presuming that in cubiclike structures it is generally small, as found, for example, for thin Ni films.[36] The different evolution of the average spin moment $m_S(t_{\mathrm{Fe,Co}})$ for the Fe and Co layers is remarkable; it indicates that their interface with the $V_2O_3(11\bar{2}0)$ layers is distinctly different. Let us recall that element-resolved hysteresis-loop measurements testify to magnetic saturation of these moments projected onto the external field parallel to the beam (Sec. II), for all thicknesses $t_{\mathrm{Fe,Co}} \leqslant 1$ nm addressed in Fig. 6. In view of its modest value ($B=1$ T, oriented at 45° to the layer normal) compared to the demagnetization fields of the ferromagnetic overlayers this points to the presence of a magnetic anisotropy in these layers, presumably of the Néel interface type due to symmetry breaking,[17] which competes with their shape anisotropy by favoring out-of-plane magnetization orientation.

As can be seen in Fig. 6, the Co overlayers are ferromagnetically ordered from the very beginning of their growth, even at room temperature, albeit with a reduced magnetic moment at the lowest thicknesses: the magnetic spin moment per atom, m_S, increases linearly with thickness up to about 1 nm to arrive at $(1.6 \pm 0.15)\mu_B$, the value of bulk hcp Co. The final observation of this value confirms the conclusion drawn from the shape of the XA spectra that Co does not form an oxide at the interface with V_2O_3. In the case of Fe, the spin part of the spontaneous magnetic moment of the layers, $m_S \times t_{\mathrm{Fe}}$, plotted as a function of their thickness t_{Fe} follows accurately a straight line, which extrapolates to zero at $t^*_{\mathrm{Fe}} = (0.21 \pm 0.02)$ nm. In other words, the spin moment per Fe atom, m_S, varies as $m_S(t_{\mathrm{Fe}}) = 2.15\mu_B - 0.45\mu_B$ nm$/t_{\mathrm{Fe}}$ and vanishes at a thickness t^*_{Fe}, which corresponds to 1 monolayer (Fig. 6). This is observed over the whole temperature range from 10 to 300 K within the experimental error. The result permits to conclude that (i) the first atomic layer of Fe on the $V_2O_3(11\bar{2}0)$ surface is nonmagnetic; (ii) as more Fe is deposited, the magnetically "dead" layer persists and the additional Fe contributes with the full bulklike moment per atom of the bcc phase, $(2.15 \pm 0.03)\mu_B$, to the spontaneous magnetization of the layers; (iii) Fe forms a smooth continuous film on $V_2O_3(11\bar{2}0)$ already for monolayer coverage; i.e., growth in the ultrathin limit proceeds essentially via the layer-by-layer mode. We note that this is not in contradiction to the morphology of the $V_2O_3(11\bar{2}0)$ surface, considering the large extension of the atomically flat terraces. The most probable epitaxial relationship is Fe (Refs. 1–10) parallel to the V_2O_3 *c* axis for Fe-layer growth with (110) orientation. The existence of the interfacial magnetically dead Fe layer provides a natural explanation for the absence of the exchange anisotropy in the $Fe/V_2O_3(11\bar{2}0)$ bilayers. Even at the low thickness of 1 atomic layer it is expected to largely reduce, if not suppress, exchange coupling across the interface. Then the interfacial exchange does not exceed the energy required to form a domain wall in the antiferromagnet, a prerequisite to generate a bias in the magnetization curve of the overlayer, as pointed out by Stamps.[5] For Co, on the other hand, the variation of the average magnetic spin moment per atom, $m_S(t_{Co})$, as $t_{Co} \rightarrow 0$ suggests that there is no

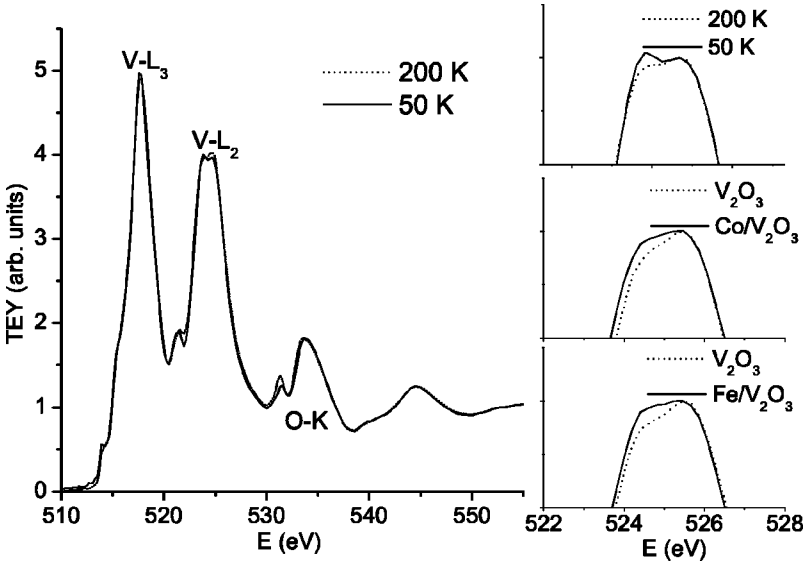

FIG. 7. XA spectrum [V $L_{2,3}(2p \rightarrow 3d)$ and O$(1s \rightarrow 2p)$ edges] of a $V_2O_3(11\bar{2}0)$ layer (thickness 80 nm) in the PM phase (200 K) and AFI phase (50 K), left panel. Right panel: details of the V L_2 edge below and above T_{MI} (top) and at 290 K after coverage with 0.5 nm Co (middle) and Fe (bottom). The spectra on the right panel are normalized to the higher-lying peak of the L_2-edge spectrum.

magnetically dead layer at the interface and that the entire film is ferromagnetic. Let us point out that the different magnetic behavior of Co as compared to Fe displayed in Fig. 6 cannot be related to different interface anisotropies that might be present in these ultrathin layers layers, as the magnetic moment projections, $m_S(t_{Fe,Co})$, are saturated in the external field applied. It is difficult to imagine that in the case of Co the increase of m_S with t_{Co} at a constant rate up to the full spin moment of hcp Co (Fig. 6) might be related to the morphology of the film in the early stage of growth. In particular, the initial formation and growth of flat islands that coalesce at $\sim$1 nm is unlikely in view of the very small temperature dependence of the spin moment between 10 and 300 K. Definite conclusions are difficult to draw. Here, further investigations are mandatory.

The reason for the presence (Fe) or absence (Co) of a magnetically dead layer at the interface of the bilayers is not obvious. Studies dealing with thin films of iron and cobalt deposited on various metallic, semiconducting, or insulating substrates have a long history. It is extensively documented that the magnetic properties of these films are sensitively linked to a rich variety of parameters, which basically mirror the well-known fundamental feature that the spontaneous magnetization of a ferromagnetic material is closely related to the nearest-neighbor coordination number, the interatomic bond length, and the nature of chemical bonding between the atoms. For itinerant magnets this translates to the form, according to the Stoner model, that the appearance of spontaneous magnetism is governed by energy gain through exchange splitting of the majority and minority spin bands.[37] A magnetic moment exists for a sufficiently large Stoner product $D(E_F) \times I$, where $D(E_F)$ is the density of states at the Fermi level and I, the Stoner factor, represents the essentially intra-atomic exchange interaction. The lateral compressive strain, suggested to be equally effective in the Fe and Co overlayers near the interface to V_2O_3 (Sec. II), presumably is to small to reduce $D(E_F)$ by broadening of the d bands due to a shorter interatomic distance and hence diminish or destabilize the spontaneous magnetic moment near the interface. It is more likely that the magnetically dead layer in the Fe film at the interface may be attributed to an electronic interaction with the oxide—i.e., to a hybridization between the Fe 3d electronic states with the V 3d and/or O 2p derived states. Electron hybridization can give rise to a charge transfer at the interface resulting in a change of $D(E_F)$ in Fe at the immediate interface such as to lift the imbalance of the electron spin-state population. Hybridization effects may be differently effective in the two bilayer systems. The differences must be associated with the specific electronic band structure of Fe and Co, making the impact of the interaction with the oxide across the interface on the magnetic moments of the FM overlayers dissimilar. This might be related to the lower Stoner factor of Fe (Ref. 37), making ferromagnetism for this metal less stable than for Co. It is obvious that calculations of the electronic structure of the two bilayer systems are required to elucidate the question why in Fe layers in contact with $V_2O_3(11\bar{2}0)$ the spontaneous magnetic moment in the first interfacial atomic layer is lost, in contrast to the case of Co.

Considering the different magnetic behavior of the ultrathin Fe and Co layers on $V_2O_3(11\bar{2}0)$, we looked, by XA spectroscopy, at the V 2p ($L_{2,3}$) and O 1s (K) edges, for signatures in the oxide of the electronic interaction with the FM films at the interfaces. Such spectra represent the density of unoccupied states of d and p character at the V and O sites, respectively, admixed into the low-lying conduction bands near the Fermi level. Deposition of Fe and Co on $V_2O_3(11\bar{2}0)$ clearly modifies the electronic structure of the oxide close to the interface, in a similar way for both ferromagnets. This is shown for the L_2-edge part of the XA spectrum of V at room temperature in Fig. 7 (right panel) for a coverage of 0.5 nm. As a reference, the complete spectra of the uncovered $V_2O_3(11\bar{2}0)$ layer in the PM metallic and AFI phase are presented (Fig. 7, left panel). We have pointed out previously[14] that the overall features of the bare $V_2O_3(11\bar{2}0)$ layer spectra are in general agreement with those of bulk V_2O_3 single crystals measured with linearly polarized x-rays;[38,39] in particular, the modifications of their shape upon crossing the PM-to-AFI phase transition show the same tendency. Small dissimilarities must be attributed to experi-

mental differences—i.e., the use of circular polarization of the x-ray beam, a different sample plane, and the inferior photon energy resolution (~0.6 eV compared to ~0.16 eV) in our study.

In the corundum structure of V_2O_3 the vanadium ions sit in an octahedron of oxygen ions. This results in an electronic structure with a $3d^2$ V^{3+} state, with two empty e_g orbitals and three t_{2g} orbitals occupied with two electrons. A small trigonal distortion causing a splitting of the $3d$-t_{2g} manifold into a nondegenerate a_{1g} orbital oriented along the c axis and two degenerate e_g^π orbitals oriented in the hexagonal plane. Strong correlations in the electronic structure pose major problems for the understanding of the oxide, even though important theoretical progress can be observed since a few years (see, for example, Refs. 9–11); this will not be addressed here. For an assignment of the different spectral features in Fig. 7 to the electronic structure of V_2O_3 and a more detailed discussion of the spectra the reader is referred to our previous publication[14] and the references therein. Let us mention that Park *et al.*,[39] in an analysis of the linear dichroism in their V $L_{2,3}$-edge XA spectra, conclude that the different phases of V_2O_3 (PM, PI, AFI) have different orbital occupations involving e_g^π e_g^π and $e_g^\pi a_{1g}$ initial states with different relative weight, such that the a_{1g} admixture decreases across the transition to the PI and AFI phases. Inherent to this is the spin and orbital dependence of the on-site $3d$-$3d$ Coulomb energy, which plays a crucial role in the metal-insulator transition. The authors argue, as already put forward by Ezhov *et al.*,[40] that the V^{3+} ions are in the $S=1$ ground state favored by the atomic Hund's rule. Note that the results of Park *et al.*[39] are well reproduced by the theory of Held *et al.*[9]

It can be seen in Fig. 7 (right panel) that the coverage of the $V_2O_3(11\bar{2}0)$ surface by Fe and Co at 290 *K* transfers spectral weight from the higher-lying peak of the double-peak V L_2 white line to the lower-lying one in a similar way for both ferromagnets, indicating a change in orbital occupation of electronic states of the oxide close to the interface. It is not surprising that the influence of the interfacial interaction on the spectral shape is small since the energy involved must be small compared to the crystal-field and on-site Coulomb interactions, which dominate the line shape of the XA spectrum.[9] The spectral evolution shows the same tendency as the corresponding spectra of the single crystal in Ref. 39 upon the transitions from the PM to the PI or AFI phases. These insulating phases have a similar electronic structure.[39,41] A comparable modification of the spectral shape occurs for the bare $V_2O_3(11\bar{2}0)$ layer at the PM-to-AFI phase transition (Fig. 7, left panel).[42] On the basis of this comparison we may conclude that the Fe and Co overlayers both induce an electronic structure in V_2O_3 near the interface, at room temperature, that resembles that of an insulating phase. This phase must be paramagnetic (the PI phase of V_2O_3) since AF order in the layers sets in near 160 K only, as reflected by the appearance of exchange bias in the $Co/V_2O_3(11\bar{2}0)$ bilayers [see Fig. 4(a)]. We suggest that the existence of the PI phase at the surface of $V_2O_3(11\bar{2}0)$ may result from an electronic interaction with Fe and Co—i.e., from hybridization of electronic states at the interface in both bilayer systems. This could modify the balance between the Coulomb interaction within the $3d$ shell of V and the hybridization of the V $3d$ and O $2p$ orbitals and thus modify the electronic properties of the oxide. Interfacial strain resulting from the lattice mismatch of the constituents is less probable as an agent since it is expected to be compressive. However, in bulk V_2O_3 the transition from the PM to the PI phase occurring, for example, by the substitution of V by Cr formally is equivalent to negative pressure.[12]

Our study reveals that exchange coupling of Co to adjacent AF $V_2O_3(11\bar{2}0)$ favors an in-plane perpendicular orientation of the magnetic moments of the two layers. However, a small canting of the AF spins is expected that should lead to a net moment—i.e., to uncompensated spins—at the interface in the antiferromagnet parallel to the F magnetization.[29,5] According to recent computer simulations, uncompensated interfacial spins anchored in the antiferromagnet[43] or uncompensated spins in the AF interior[44] are believed to be responsible for the exchange bias in F/AF-layered systems. There is new evidence for such link: Ohldag *et al.*[45] performing XMCD experiments on different exchange-bias sandwiches with Co observed uncompensated interfacial spins locked in the antiferromagnet that do not follow the external field. They constitute only a fraction of a monolayer and are shown, in an extension of the classical Meiklejohn-Bean model,[46] to account for the exchange bias effect in these systems. Efforts to resolve a XMCD signal at the $L_{2,3}$ edges of V in $Co/V_2O_3(11\bar{2}0)$ bilayers at temperatures below T_N were not successful; i.e., uncompensated V $3d$ spins in AF V_2O_3 could not be detected. We estimate that a dichroic signals, if existing, must be below 1% of the isotropic signal. Similarly, searching for a dichroic signal at the V $L_{2,3}$ edges above T_N was just as negative. Hence there is no evidence of magnetic order on the V $3d$ states induced in PI V_2O_3 by exchange interaction or electron hybridization at the interface with Co. In fact the lack of hybridization-induced spin polarization may not be surprising as the V magnetic moment is almost entirely due to electrons in e_g^π orbitals oriented in the (0001) plane of the oxide[47] while the V orbitals relevant for hybridization with Co in the $(11\bar{2}0)$ plane are of a_{1g} symmetry.

IV. SUMMARY

Epitaxial films of V_2O_3 on $(11\bar{2}0)$-oriented sapphire are used as substrates for thin films of Fe and Co. X-ray diffraction indicates textured growth of the overlayers with bcc (110) and hcp (0001) orientations, respectively. Special properties of the oxide films are a stripelike surface structure perpendicular to the c axis of the rhombohedral lattice with extended atomically flat terraces and a transition from a paramagnetic metallic to an antiferromagnetic insulating phase at $T_{MI}=T_N=160$ K. The magnetic properties of both ferromagnets are determined by the interaction across the interface with the oxide and its surface morphology. The faceted V_2O_3 surface induces a uniaxial magnetic anisotropy with magnetocrystalline and magnetostatic contibutions, similarly as observed for ferromagnetic films on stepped surfaces. Cooling the bilayers in a magnetic field to below T_N produces an

exchange bias for the hysteresis loops of the Co layers, but not for the Fe layers. This is a manifestation of a different interaction at the interface with the adjacent oxide. Measurements of XMCD support the view that this difference between the two ferromagnets results from a magnetically dead atomic Fe layer at the interface, which suppresses the F/AF exchange interaction. The microscopic origin of the dead layer remains an open question. Remarkably, XA spectroscopy at the V 2*p* threshold by TEY detection reveals that both F overlayers induce a paramagnetic insulating phase in the V_2O_3 substrate at the interface. This can be been concluded from a comparison with the corresponding spectra of bulk V_2O_3 single crystals doped with Cr. Oxide formation in the ferromagnets at the interface can excluded.

ACKNOWLEDGMENTS

We acknowledge helpful discussions with K. Samwer. The work was supported by the Deutsche Forschungsgemeinschaft within SFB 602. It has benefited from the Access to Large Facilities Activity of the European Community's TMR Program. We thank S. Janicot at LURE for technical support.

[1] J. B. Kortright, D. D. Awschalom, J. Stöhr, S. D. Bader, Y. U. Idzerda, S. S. P. Parkin, I. K. Schuller, and H. C. Siegmann, J. Magn. Magn. Mater. **207**, 7 (1999).
[2] G. A. Prinz, Science **282**, 1660 (1998).
[3] J. Nogués and I. K. Schuller, J. Magn. Magn. Mater. **192**, 203 (1999).
[4] A. E. Berkowitz and K. Takano, J. Magn. Magn. Mater. **200**, 552 (1999).
[5] R. L. Stamps, J. Phys. D **33**, R247 (2000).
[6] *Spin Electronics*, edited by M. Ziese and M. J. Thornton, Springer Lecture Notes in Physics Vol. 569 (Springer, Berlin, 2001).
[7] M. R. Fitzsimmons, S. D. Bader, J. A. Borchers, G. P. Felcher, J. K. Furdyna, A. Hoffmann, J. B. Kortright, I. K. Schuller, T. C. Schulthess, S. K. Sinha, M. F. Toney, D. Weller, and S. Wolf, J. Magn. Magn. Mater. **271**, 103 (2004).
[8] M. Imada, A. Fujimori, and Y. Tokura, Rev. Mod. Phys. **70**, 1039 (1998).
[9] K. Held, G. Keller, V. Eyert, D. Vollhardt, and V. I. Anisimov, Phys. Rev. Lett. **86**, 5345 (2001).
[10] R. Shiina, F. Mila, F. C. Zhang, and T. M. Rice, Phys. Rev. B **63**, 144422 (2001).
[11] A. Tanaka, J. Phys. Soc. Jpn. **71**, 1091 (2002).
[12] D. B. McWhan, J. P. Remeika, T. M. Rice, W. F. Brinkman, J. P. Maita, and A. Menth, Phys. Rev. Lett. **27**, 941 (1971).
[13] R. M. Moon, Phys. Rev. Lett. **25**, 527 (1970); R. E. Word, S. A. Werner, W. B. Yelon, J. M. Honig, and S. Shivashankar, Phys. Rev. B **23**, 3533 (1981); W. Bao, C. Broholm, S. A. Carter, T. F. Rosenbaum, G. Aeppli, S. F. Trevino, P. Metcalf, J. M. Honig, and J. Spalek, Phys. Rev. Lett. **71**, 766 (1993).
[14] B. Sass, C. Tusche, W. Felsch, N. Quaas, A. Weismann, and M. Wenderoth, J. Phys.: Condens. Matter **16**, 77 (2004).
[15] E. Goering, A. Fuss, W. Weber, J. Will, and G. Schütz, J. Appl. Phys. **88**, 5920 (2000).
[16] R. Nakajima, J. Stöhr, and Y. Idzerda, Phys. Rev. B **59**, 6421 (1999).
[17] L. Néel, J. Phys. Radium **15**, 225 (1954).
[18] B. Hillebrands, P. Baumgart, and G. Güntherodt, Phys. Rev. B **36**, 2450 (1987).
[19] M. Albrecht, T. Furubayashi, M. Przybylski, J. Korecki, and U. Gradmann, J. Magn. Magn. Mater. **113**, 07 (1992).
[20] D. S. Chuang, C. A. Ballentine, and R. C. O'Handley, Phys. Rev. B **49**, 15 084 (1994).
[21] R. K. Kawakami, E. J. Escoria-Aparicio, and Z. Q. Qiu, Phys. Rev. Lett. **77**, 2570 (1996); R. K. Kawakami, M. O. Bowen, H. J. Choi, E. J. Escoria-Aparicio, and Z. Q. Qiu, Phys. Rev. B **58**, R5924 (1998).
[22] R. A. Hyman, A. Zangwill, and M. D. Stiles, Phys. Rev. B **58**, 9276 (1998).
[23] P. Krams, B. Hillebrands, A. Güntherodt, and H. P. Oepen, Phys. Rev. B **49**, 3633 (1994).
[24] R. Arias and and D. L. Mills, Phys. Rev. B **59**, 11 871 (1999).
[25] J. H. Wolfe, R. K. Kawakami, W. L. Ling, Z. Q. Qiu, R. Arias, and D. L. Mills, J. Magn. Magn. Mater. **232**, 36 (2001) and references cited therein.
[26] S. Dubourg, J. F. Bobo, B. Warot, E. Snoeck, and J. C. Ousset, Phys. Rev. B **64**, 054416 (2001).
[27] Disregarding these small differences, the angles α_1 and α_2 are close to 90° for magnetization reversal in the hard direction regarded here. This means that they are not really chosen freely, leaving the anisotropy constants K_1 and K_2 as the only free essential parameters in the fit of the magnetization curves.
[28] C. Tusche, Diplomarbeit, Universität Göttingen, 2003.
[29] N. C. Koon, Phys. Rev. Lett. **78**, 4865 (1997).
[30] T. C. Schulthess and W. H. Butler, Phys. Rev. Lett. **81**, 4516 (1998); J. Appl. Phys. **85**, 5510 (1999).
[31] D. Mauri, H. C. Siegmann, P. S. Bagus, and E. Kay, J. Appl. Phys. **62**, 3047 (1987).
[32] E. J. Escorcia-Aparicio, H. J. Choi, W. L. Ling, R. K. Kawakami, and Z. Q. Qiu, Phys. Rev. Lett. **81**, 2144 (1998).
[33] T. J. Regan, H. Ohldag, C. Stamm, F. Nolting, J. Lüning, J. Stöhr, and R. L. White, Phys. Rev. B **64**, 214422 (2001); J. van Elp and B. G. Searle, J. Electron Spectrosc. Relat. Phenom. **86**, 93 (1997); J. P. Crocombette, M. Pollak, F. Jollet, N. Thromat, and M. Gautier-Soyer, Phys. Rev. B **52**, 3143 (1995).
[34] B. T. Thole, P. Carra, F. Sette, and G. van der Laan, Phys. Rev. Lett. **68**, 1943 (1992); P. Carra, B. T. Thole, M. Altarelli, and X. Wang, *ibid.* **70**, 694 (1993).
[35] C. T. Chen, Y. U. Idzerda, H.-J. Lin, N. V. Smith, G. Meigs, E. Chaban, G. H. Ho, E. Pellegrin, and F. Sette, Phys. Rev. Lett. **75**, 152 (1995).
[36] F. Wilhelm, P. Poulopoulos, P. Srivastava, H. Wende, M. Farle, K. Baberschke, M. Angelakeris, N. K. Flevaris, W. Grange, J. P. Kappler, G. Ghiringhelli, and N. B. Brookes, Phys. Rev. B **61**, 8647 (2000).
[37] J. Kübler, *Theory of Itinerant Electron Magnetism* (Clarendon Press, Oxford, 2000).

[38] O. Müller, J. P. Urbach, G. Goering, T. Weber, R. Barth, H. Schuler, M. Klemm, S. Horn, and M. L. denBoer, Phys. Rev. B **56**, 15 056 (1997).

[39] J. H. Park, L. H. Tjeng, A. Tanaka, J. W. Allen, C. T. Chen, P. Metcalf, J. M. Honig, F.-M. F. de Groot, and G. A. Sawatzky, Phys. Rev. B **61**, 11 506 (2000).

[40] S. Yu. Ezhov, V. I. Anisimov, D. I. Khomskii, and G. A. Sawatzky, Phys. Rev. Lett. **83**, 4136 (1999).

[41] P. Pfalzer, J. Will, A. Nateprov, Jr., M. Klemm, V. Eyert, S. Horn, A. I. Frenkel, S. Calvin, and M. L. denBoer, Phys. Rev. B **66**, 085119 (2002).

[42] The spectral change is more pronounced in the latter case (Fig. 7, right panel), but this can be attributed to the fact that the probing depth of the x rays exceeds the region at the surface of V_2O_3 modified by the interaction with the Fe and Co overlayers. This means that the measured XA spectrum of the bilayers contains a contribution of nonmodified V_2O_3 within the probing depth somewhat underneath the surface.

[43] K. Takano, R. H. Kodama, A. E. Berkowitz, W. Cao, and G. Thomas, Phys. Rev. Lett. **79**, 1130 (1997).

[44] U. Nowak, A. Misra, and K. D. Usadel, J. Magn. Magn. Mater. **249**, 243 (2002).

[45] H. Ohldag, A. Scholl, F. Nolting, A. Ahrenholz, S. Maat, A. T. Young, M. Carey, and J. Stöhr, Phys. Rev. Lett. **91**, 017203 (2003).

[46] W. H. Meiklejohn and C. P. Bean, Phys. Rev. **105**, 904 (1957).

[47] P. J. Brown, M. M. R. Costa, and K. R. A. Ziebeck, J. Phys.: Condens. Matter **10**, 9581 (1998).